

Spectral-reflectance linear models for optical color-pattern recognition

Juan L. Nieves, Javier Hernández-Andrés, Eva Valero, and Javier Romero

We propose a new method of color-pattern recognition by optical correlation that uses a linear description of spectral reflectance functions and the spectral power distribution of illuminants that contains few parameters. We report on a method of preprocessing color input scenes in which the spectral functions are derived from linear models based on principal-component analysis. This multichannel algorithm transforms the red–green–blue (RGB) components into a new set of components that permit a generalization of the matched filter operations that are usually applied in optical pattern recognition with more-stable results under changes in illumination in the source images. The correlation is made in the subspace spanned by the coefficients that describe all reflectances according to a suitable basis for linear representation. First we illustrate the method in a control experiment in which the scenes are captured under known conditions of illumination. The discrimination capability of the algorithm improves upon the conventional RGB multichannel decomposition used in optical correlators when scenes are captured under different illuminant conditions and is slightly better than color recognition based on uniform color spaces (e.g., the CIE Lab system). Then we test the coefficient method in situations in which the target is captured under a reference illuminant and the scene that contains the target under an unknown spectrally different illuminant. We show that the method prevents false alarms caused by changes in the illuminant and that only two coefficients suffice to discriminate polychromatic objects. © 2004 Optical Society of America

OCIS codes: 100.5010, 330.1690, 100.4550.

1. Introduction

In addition to shape and size, color is one of the most important characteristics in the discrimination and recognition of objects. The introduction of color information in pattern recognition by optical correlation is usually made by means of a multichannel correlation technique that decomposes the source and the target color images in three [red–green–blue (RGB)] channels.^{1–4} The correlation is made separately for each channel, and arithmetic or logical point-wise operations can be used to derive the final output. A common way in which objects are optically recognized is by use of a multichannel joint-transform correlator in which a filter matched to the target is used in each channel.⁵

Different methods to enhance the differences be-

tween the images of the channels to achieve better recognition have been proposed.^{6–8} Some of these transformations benefit color-vision models and transform the color channels into three color signals that correspond to one achromatic channel—the luminance channel—and two opponent channels—the red–green and the blue–yellow channels.⁷ This method increases discriminability when it is compared with the RGB transformation and even reduces the number of effective channels that contribute to color correlation, with the two opponent channels being sufficient for good color correlation. The use of color transformations that are not based on human visual models has also been effective in increasing the discrimination of color objects and preventing false alarms for objects that are equal in shape but different in color.⁸ An alternative way to include color information in optical pattern recognition is by the use of the three-dimensional (3D) color correlation.^{9,10} The colors of images are introduced as a third dimension in addition to spatial variables, and thus a 3D Fourier transform can be defined. The technique encodes 3D functions onto two-dimensional functions and leads to new encoding proposals in optical correlators.¹¹

The authors are with the Departamento de Óptica, Facultad de Ciencias, Universidad de Granada, 18071-Granada, Spain. J. L. Nieves's e-mail address is jnieves@ugr.es.

Received 30 May 2003; revised manuscript received 16 September 2003; accepted 8 December 2003.

0003-6935/04/091880-12\$15.00/0

© 2004 Optical Society of America

Although satisfactory results can be obtained with the techniques described above, changes in the illuminant may cause difficulties in recognizing color objects. Only a few studies that address the problem of finding optical pattern-recognition architectures that are not susceptible to changes in the illuminant have been published.^{12,13} In one of these publications¹² the use of uniform color spaces, which are more stable in the face of these changes, is considered. For common illuminants the transformation from RGB to the coordinates of the CIELAB system allows us to overcome some of the recognition difficulties that occur when there is a change in the illuminant that we have mentioned. The correlation made among luminance, chroma, and hue channels provides better discrimination than conventional RGB techniques. The drawback of the method is that the matrices that transform the RGB values to the XYZ tristimulus values depend on the particular choice of illumination (i.e., the spectral power distribution of the light source). But the use of only two channels (the luminance and the hue channels) simplifies recognition and leads to pattern recognition results that are stable when the illuminant changes.

Color objects can be also recognized based on computational algorithms that are color constant. Color indexing involves matching color-space histograms and departs from other recognition techniques based on the geometrical properties of objects.¹⁴ One identifies objects by comparing their color components with the color components of each object in a previously defined database; the intersection of histograms is usually used to recognize the color object. Before histogramming, illuminant-invariant descriptors can be defined to derive pattern recognition independently of changes of illuminant.¹⁵ Whereas optical pattern recognition seeks correlation peaks that correspond to the spatial position of the target in the image, computational color-constancy algorithms usually recover an illuminant-independent representation of the color images or the retrieval of images from large collections of image databases.¹⁵⁻¹⁷

The study presented here describes what is to our knowledge a new method of optical color-pattern recognition that leads to discrimination results that are independent of the spectral changes of the illuminant under which an image is captured. It is a multichannel algorithm that uses a linear model based on principal-component analysis (PCA), which represents the spectral reflectance function of each image pixel on a suitable basis for linear representation. A correlation is then made throughout the spatial distribution of the coefficients derived from the linear representation of each reflectance function. When the illuminant is unknown, or when it is difficult to obtain a spectroradiometric measurement of it, we used an illuminant-estimation hypothesis before making the correlation. The method is tested with various test illuminants and compared with the multichannel RGB and CIELab techniques; an improvement in the discrimination capability of optical color-pattern recognition is shown when the target is

captured under one illuminant and the source under a spectrally different and *a priori* unknown illuminant.

2. Linear Description of Surfaces and Illuminants in Color Images

Let us assume a scene viewed under a given illumination and captured by a color camera. According to basic concepts of image acquisition, the intensity of each image pixel can be expressed as

$$I_N(x, y) = \sum_{\lambda} q_N(\lambda) S(x, y, \lambda) E(x, y, \lambda) \Delta\lambda, \quad (1)$$

where N represents each of the channels that capture the color image [e.g., $N = 3$ for conventional CCD color cameras with three channels (R, G, and B)], $q_N(\lambda)$ is the spectral sensitivity of each channel, $S(x, y, \lambda)$ is the spectral reflectance function of the pixel (x, y), and $E(x, y, \lambda)$ is the spectral power distribution (SPD) of the illuminant under which the image is captured at pixel (x, y). We assume that the image is uniformly illuminated, and thus in Eq. (1) we substitute $E(\lambda)$, which does not depend upon pixel coordinates, for $E(x, y, \lambda)$.

It is possible to find¹⁸ square-integrable functions $S_j(\lambda)$ ($j = 1, 2, \dots$) such that for any surface reflectance $S(x, y, \lambda)$ there is a single set of real numbers $\sigma_j(x, y)$, and thus

$$S(x, y, \lambda) = \sum_{j=1}^n \sigma_j(x, y) S_j(\lambda). \quad (2)$$

The $S_j(\lambda)$ functions form a basis of linear function space \mathbf{L}^2 and allow the function $S(x, y, \lambda)$ to be represented by the vector of coefficients $\sigma^{xy} = [\sigma_1^{xy}, \dots, \sigma_n^{xy}]$. We can act in a similar way and find square-integrable functions $E_i(\lambda)$ ($i = 1, 2, \dots$) such that for any SPD of illuminant $E(\lambda)$ there is a single set of real numbers, ϵ_i , and thus

$$E(\lambda) = \sum_{i=1}^m \epsilon_i E_i(\lambda), \quad (3)$$

where we have assumed that the illumination is spatially uniform. The $E_i(\lambda)$ functions allow SPD $E(\lambda)$ to be represented by the vector of coefficients $\epsilon = [\epsilon_1, \dots, \epsilon_m]$. It should be noted that, whereas the spectral reflectance function and the SPD of the illuminant depend on the wavelength, coefficients σ_j^{xy} and ϵ_i do not; coefficients σ_j^{xy} vary only in relation to spatial coordinates (x, y). By incorporating Eq. (2) into Eq. (1) we can express the intensity of the multichannel image as

$$I_N(x, y) = \sum_{i=1}^m \sum_{j=1}^n \sigma_j(x, y) \epsilon_i \gamma_{ijN}, \quad (4)$$

where the factor $\gamma_{ijN} = \sum_{\lambda} q_N(\lambda) S_j(\lambda) E_i(\lambda) \Delta\lambda$ contains only fixed elements that are independent of the image captured once the bases of linear representation have been selected. Most of the spectral reflectance functions and SPDs of illuminants can be described by small-dimensional linear models; earlier studies

have shown that five to seven eigenvectors suffice for adequate reconstructions of surfaces,^{18–21} and only three to five are required for illuminants.^{22–24} The algorithm that we have developed here will use only three eigenvectors for surfaces and illuminants. This economy is of particular interest when we capture the input images with a CCD color camera. The selection of 3D linear models is imposed by the fact that if we had three RGB values we thus needed three eigenvalues to ensure correspondence between the camera responses and the number of eigenvectors. Better representations could have been obtained with a greater number of eigenvectors, but our election was a compromise between more-accurate spectral representations and lower computational costs (remember that the purpose of the recognition algorithm is to obtain a correlation peak and not to recover an illuminant-independent image similar to the original image).

3. Outline of the Color-Correlation Method

The originality of the study presented here lies in the use of linear models in optical color-pattern recognition. The linear models are derived from PCA, which represents the spectral reflectance function of each image pixel and the SPD of the illuminant on suitable bases. The linear description of surfaces and illuminants is well documented in the literature, but until now, and to our knowledge, this linear description of spectral functions has not been applied in multichannel optical correlation for color-pattern recognition. We propose to implement the correlation throughout the spatial distribution of coefficients σ_j^{xy} derived from the linear representations of the reflectance functions because these coefficients vary only in relation to the spatial coordinates. Previously we needed to express the intensity of each image pixel according to Eq. (4), which would imply the election of the basis functions $S_j(\lambda)$ and $E_i(\lambda)$ for an adequate representation of the spectral reflectance functions and the SPD of the illuminant.

Let us consider first, to illustrate the algorithm's performance, the trivial case in which the illuminant is known. In this case we can always get the coefficient σ_j^{xy} that determines each surface reflectance simply by solving the linear equation set of Eq. (4). This process can be reduced to a matrix inversion when the number of channels that specifies the image is $N = n$; i.e.,

$$\sigma^{xy} = \gamma^{-1} I^{xy}, \quad (5)$$

where the quantities on the right-hand side of Eq. (5) are all known. We propose to transform the source and the target color images according to Eq. (5). Based on this transformation, recognition can be achieved from the finite subspace of the σ^{xy} coefficients, and the matched filter operations that are usually applied in optical pattern recognition can be generalized. Let $\sigma_s(x, y)$ and $\sigma_t(x, y)$ represent the input coefficients associated with the transformed source image and the impulse response of a Fourier

filter associated with the target to be discriminated, respectively. The correlation between the transformed color image and the filter impulse response is defined as

$$c_\sigma(x, y, j) = \sum_{x'=0}^{dx-1} \sum_{y'=0}^{dy-1} \sigma_s(x, y, j) \sigma_t^*(x' - x, y' - y, j) \quad (j = 1 \dots n), \quad (6)$$

where dx and dy are the dimensions of the image and j is the number of channels (dimension of the surface reflectance basis), which are processed independently.

It is difficult to handle this trivial case with real images for which the SPD of illumination can be known only from spectroradiometric measurements, but it illustrates quite well how the multichannel transformation allows us to preserve the spatial information of the image (shape, size, etc.) and avoid any dependence on the spectral characteristics of the illumination. Nevertheless, in other situations it is clear from Eq. (4) that we need an estimation algorithm of the illumination—what it is usually called an illuminant estimation hypothesis—in the scene to solve for coefficients σ_j^{xy} . The use of the optical correlation method proposed here could potentially be a color-pattern-recognition technique that is invariant to changes in the illuminant, either *a priori* known or unknown.

4. Illuminant-Estimation Hypothesis

There are several ways to get information about the illumination and to reduce the uncertainty of Eq. (4). The illuminant-estimation approaches that have been used in various color-constancy algorithms make use of scene averages, highlights, shadows, mutual illumination, or subspace constraints.^{18,25–28} The purpose of our study is not to develop a color-constancy image but to benefit from these color-constancy algorithms to obtain correlation peaks that do not vary when the illuminant changes. So we consider one of the simplest illuminant-estimation hypotheses found in the literature to test the correlation results derived from the multichannel transformation associated with Eq. (5) because it suffices to produce good discrimination results by optical correlation. This hypothesis makes use of a reference white, which will be a diffuse white surface and must be placed within the scene to be captured. Following the linear description of surfaces and illuminants derived from Eqs. (1)–(4), the intensity of the multichannel image of the white surface can be expressed as

$$I_{N,W}(x, y) = \sum_{\lambda} \sum_{i=1}^m S_W(x, y, \lambda) \varepsilon_i E_i(\lambda) q_N(\lambda) \Delta\lambda \\ = \sum_{i=1}^m \varepsilon_i \left[\sum_{\lambda} S_W(x, y, \lambda) E_i(\lambda) q_N(\lambda) \Delta\lambda \right], \quad (7)$$

where $S_W(x, y, \lambda)$ is the *a priori* known reflectance of the white surface placed at coordinates (x, y) . The factor in brackets contains only fixed elements, which are independent of the image once a suitable basis for linear representation of illuminants has been selected. The quantities $I_{N,W}(x, y)$ are all known from the location of the white surface in the captured image.

Thus, if the number of channels that specifies the image is $N = m$, the linear system of Eq. (7) can be solved for each ϵ_i . By substituting the obtained coefficients ϵ_i into Eq. (4) we can recover the coefficient σ_j^{xy} for each image pixel as

$$\sigma^{xy} = \Lambda_\epsilon^{-1} I^{xy}, \quad (8)$$

where $\Lambda_\epsilon = \sum_{i=1}^m \epsilon_i \gamma_{ijN}$ is the $N \times m$ lighting matrix derived from the illuminant-estimation algorithm. This equation is analogous to Eq. (5) and allows us to derive a multichannel representation of the image that does not depend on the spectral changes in the illumination under which the image is captured.

5. Results

To demonstrate the possibilities of using the linear models in optical color-pattern recognition, first we show in Subsection 5.A the results derived from a control experiment in which the spectral power distribution of the illuminant is known *a priori*. The discrimination capability of the method is compared with that derived from RGB and CIELab multichannel decompositions. Next, in Subsection 5.B we apply the illuminant-estimation hypothesis to obtain color correlation under conditions of unknown illuminant. Last, in Subsection 5.C we show an example of the discrimination results derived from an outdoor color scene that was captured under daylight illumination.

A. Control Experiment when the Illuminant was Known

Let us take the scene in Fig. 1 in which object O1 is the target when the scene is captured under illuminant D65, which is chosen here as the reference illuminant. The colored areas of the target (and of the scene also) reproduce different objects from the GretagMacbeth ColorChecker chart. Inasmuch as optical correlation depends strongly on the spatial characteristics of the objects to be discriminated, objects O1–O4 were all of the same shape but different in color (see Table 1). In addition, the colored areas of object O4 were selected in such a way that the differences in RGB values compared with those of O1 were small under each of the test illuminants. The RGB components of each color area that composes each object and the RGB color differences are listed in Table 2. The color areas of objects O1 and O4 were chosen such that it was difficult to discriminate these two color objects under the different illuminant con-

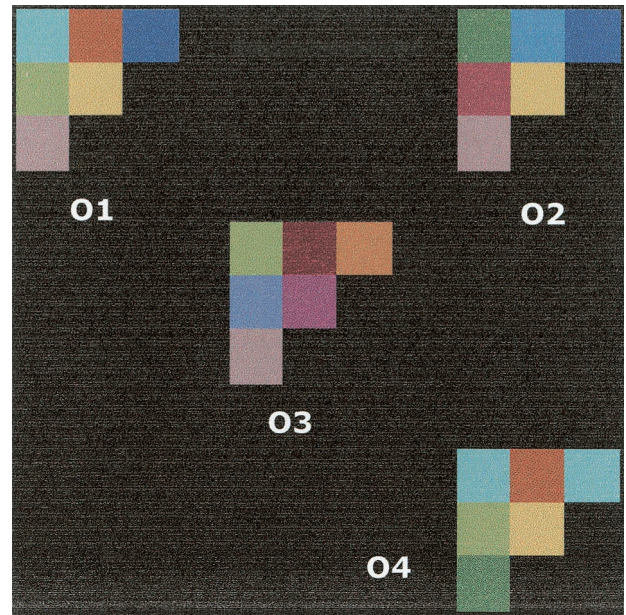


Fig. 1. Input color image captured under illuminant D65. Object O1 was the target when the scene was captured under this illuminant.

ditions. The RGB color difference was calculated from the formula

$$\Delta\text{RGB} = [(\bar{R}_1 - \bar{R}_i)^2 + (\bar{G}_1 - \bar{G}_i)^2 + (\bar{B}_1 - \bar{B}_i)^2]^{1/2} \quad (i = 2, 3, 4),$$

where we obtained \bar{R} , \bar{G} , and \bar{B} by averaging the RGB color components of the six color areas that compose objects O1–O4.

We made a simulation in which the scene in Fig. 1 was captured with a CCD color camera (JVC TK-1270E), and thus $N = 3$ in the following calculations [Fig. 2(a)]. The scene was captured under four test illuminants: D65, A, 10,000 K, and a simulated orange illuminant that corresponds to equienergy light filtered by an orange plastic filter [Fig. 2(b)]. The $S_j(\lambda)$ basis functions were obtained first through a PCA of the 24 surface reflectance functions of the ColorChecker. The dimension of the basis was fixed at $n = 3$, which corresponds to the number of RGB channels. Then we used Eq. (4) to transform both the target under the reference illuminant and the source image under each of the test illuminants. We performed three numerical correlations: First, we used the conventional RGB multichannel decomposition, which transformed the color images into the three color channels R, G, and B.³ Second, we used the CIELab multichannel decomposition¹³; for each of the illuminants a linear transformation from the RGB values to CIELab coordinates was derived,²⁹ and then the source and the target were transformed to three color components, L^* , a^* , and b^* . Third, we performed our multichannel decomposition expressed in terms of three coefficients, σ_1^{xy} , σ_2^{xy} , and σ_3^{xy} . In all cases the correlation was made separately for each channel and the AND logic operator was

Table 1. RGB Components of the Six Color Areas of Objects O1–O4 under the D65 Illuminant^a

Object	R						G						B					
O1	64	96	29	70	137	97	126	42	37	104	125	78	130	22	74	53	56	78
O2	28	30	29	78	137	97	68	73	37	29	125	78	41	107	74	35	56	78
O3	70	57	112	60	80	97	104	14	73	68	37	78	53	16	34	102	65	78
O4	64	96	64	70	137	28	126	42	126	104	125	68	130	22	130	53	56	41

^aFrom left to right for each R, G, and B component, the column values correspond to each of the six color areas that compose objects O1–O4.

applied with the usual threshold of 50% of the maximum as the positive discrimination threshold.

The results of the three approaches are summarized in Tables 3–5. With the RGB multichannel correlation, both O1 and O4 are identified as targets for all test illuminants. Even under the reference illuminant the RGB decomposition experienced problems with the discrimination of object O1. There were also false alarms between objects O1 and O3 under the orange illuminant. The correlation based on the CIE Lab system improved the RGB results and prevented all the false alarms except that for O4 under the A illuminant. The method of coefficient correlation, however, provided enough discrimination for recognition of O1 under each test illuminant without errors. An example of the results derived from correlation coefficients σ_1^{xy} , σ_2^{xy} , and σ_3^{xy} is set out in Fig. 3, which shows the correlation peaks obtained when the scene was captured under illuminant A.

The results also suggest that the greater the number of basis vectors selected to represent each reflectance, the better the method's discrimination capability. When PCA is used to describe the data, the first basis vector $S_1(\lambda)$ is related to the mean of $S(\lambda)$. This could explain why correlation coefficient σ_1^{xy} fails to identify any difference between the source and the target objects. Thus an application of the AND logic operator to only two parameters alone, the σ_2^{xy} and σ_3^{xy} coefficients, permits discrimination of the target. This result also coincides with the CIE Lab results because it is enough to use only the a^* and b^* coordinates to recognize the target under all illuminant conditions. In this way it is possible to reduce the computation time in color recognition when the targets or the sources are chromatically complex. Because there is considerable evidence that PCA provides a reasonable description of many surfaces with a small number of basis vectors

Table 2. RGB Color Difference ΔRGB between Color Object O1 Captured under the D65 Illuminant and Objects O2–O4 Captured under Each of the Test Illuminants

Test Illuminant	Color Difference ΔRGB		
	Object O2	Object O3	Object O4
D65	23	26	15
A	61	62	43
10,000K	57	57	40
Orange	22	32	21

($n = 3 \dots 7$),^{18–21} we could expand this analysis to higher-order coefficients such as σ_4^{xy} and σ_5^{xy} . Therefore the correlation expressed by Eq. (6) could be extended to more than three coefficients to derive a set of correlation planes $c_\sigma(x, y, j)$ of the desirable dimension $j = n$. This ability gives our technique a great advantage compared with other multichannel techniques because we are not limited to only three color components (i.e., the RGB values or the $L^*a^*b^*$ coordinates) for performing optical recognition. In

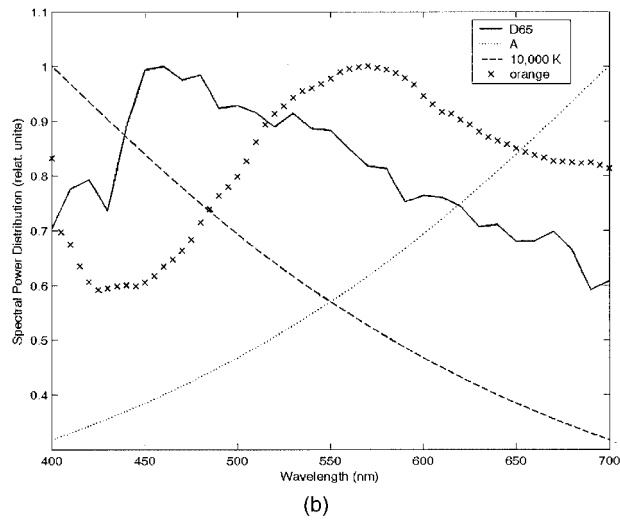
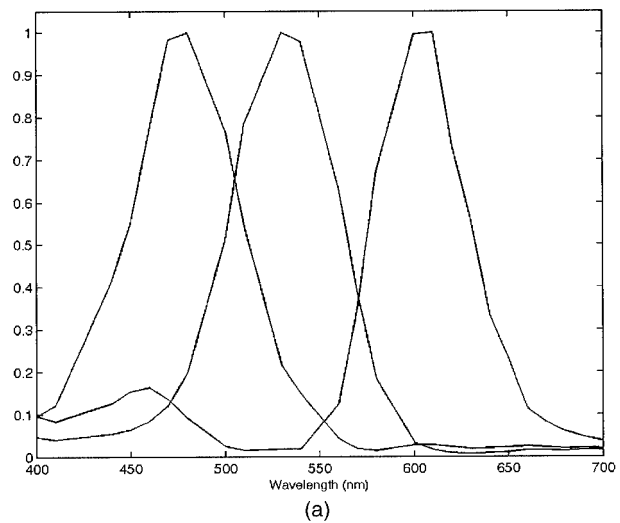


Fig. 2. (a) Normalized spectral sensitivity of the three sensors, R, G, and B, of the JVC TK-1270E camera. (b) Spectral power distributions of test illuminants D65, A, 10,000 K, and orange.

Table 3. Correlation and Discrimination Results Obtained from Conventional RGB Multichannel Decomposition under Known Illuminant Conditions^a

Illuminant	Channel	Object				50% Threshold
		O1	O2	O3	O4	
D65	R	3.647×10^{14}	2.517×10^{14}	2.360×10^{14}	2.793×10^{14}	1.824×10^{14}
	G	4.311×10^{14}	2.323×10^{14}	1.917×10^{14}	4.760×10^{14}	2.380×10^{14}
	B	2.127×10^{14}	9.851×10^{13}	1.026×10^{14}	2.165×10^{14}	1.083×10^{14}
Recognized	AND	Yes	No	No	Yes	
A	R	3.096×10^{14}	2.099×10^{14}	2.058×10^{14}	2.319×10^{14}	1.548×10^{14}
	G	1.616×10^{14}	8.748×10^{13}	7.114×10^{13}	1.770×10^{14}	8.852×10^{13}
	B	4.906×10^{13}	2.426×10^{13}	2.735×10^{13}	5.305×10^{13}	2.652×10^{13}
Recognized	AND	Yes	No	No	Yes	
10,000K	R	1.413×10^{14}	9.979×10^{13}	9.440×10^{13}	1.082×10^{14}	7.065×10^{13}
	G	2.058×10^{14}	1.108×10^{14}	9.405×10^{13}	2.260×10^{14}	1.130×10^{14}
	B	1.252×10^{14}	6.094×10^{13}	6.322×10^{13}	1.318×10^{14}	6.590×10^{13}
Recognized	AND	Yes	No	No	Yes	
Orange	R	5.252×10^{14}	3.531×10^{14}	3.274×10^{14}	4.036×10^{14}	2.626×10^{14}
	G	4.672×10^{14}	2.523×10^{14}	2.588×10^{15}	5.175×10^{14}	2.588×10^{14}
	B	1.344×10^{14}	6.656×10^{13}	7.272×10^{13}	1.481×10^{14}	5.740×10^{13}
Recognized	AND	Yes	No	Yes	Yes	

^aThe target is object O1 under illuminant D65.

this case it is clear that additional RGB components are required in Eq. (7) for solution of the coefficients [e.g., use of six digital counts $I_N(x, y)$ per pixel allows for the use of six eigenvectors for spectral reconstruction].³⁰ It is a matter for further studies to consider multifilter trichromatic image devices that allow the use of more than three eigenvectors to reconstruct spectra and the application of these devices to optical pattern recognition.

B. Correlation Results When the Illuminant was Unknown
When the illuminant conditions were unknown we applied the reference surface algorithm explained in

Section 4. The reference surface was placed in the lower left corner of the scene, as shown in Fig. 4, and intensity $I_{N,W}$ of the corresponding image pixels was captured. The white reference surface was chip number 19 of the GretagMacbeth ColorChecker. As in the previous case, object O1 was the target when the scene was captured under illuminant D65, and the scene was captured under four unknown test illuminants, which are were assumed to be characterized by a broadband and smoothed spectrum.

The first step in solving Eq. (4) was selection of appropriate basis functions $E_i(\lambda)$ for any SPD of the illuminants. A set of 83 SPDs of illuminants that

Table 4. Correlation and Discrimination Results Obtained from Multichannel Decomposition Based on the CIE Lab Color Transformation under Known Illuminant Conditions^a

Illuminant	Channel	Object				50% Threshold
		O1	O2	O3	O4	
D65	L^*	1.246×10^{11}	8.977×10^{10}	7.685×10^{10}	1.320×10^{11}	6.814×10^{10}
	a^*	5.564×10^{12}	1.251×10^{12}	1.538×10^{12}	4.219×10^{12}	2.782×10^{12}
	b^*	2.969×10^8	7.672×10^7	1.157×10^8	1.004×10^8	1.485×10^8
Recognized	AND	Yes	No	No	No	
A	L^*	1.313×10^{13}	1.072×10^{13}	9.742×10^{12}	1.279×10^{13}	6.566×10^{12}
	a^*	1.430×10^{14}	2.984×10^{13}	3.490×10^{13}	1.098×10^{14}	7.149×10^{13}
	b^*	6.505×10^9	2.627×10^9	3.485×10^9	3.262×10^8	3.253×10^9
Recognized	AND	Yes	No	No	Yes	
10,000K	L^*	9.757×10^3	9.896×10^3	9.963×10^3	9.768×10^3	5.228×10^3
	a^*	5.705×10^2	1.279×10^2	2.000×10^2	4.517×10^2	2.852×10^2
	b^*	3.800×10^2	1.510×10^2	8.100×10^3	1.250×10^2	1.900×10^2
Recognized	AND	Yes	No	No	No	
Orange	L^*	1.234×10^{13}	1.003×10^{13}	9.408×10^{12}	1.212×10^{13}	6.169×10^{12}
	a^*	1.333×10^{14}	2.669×10^{13}	3.652×10^{13}	9.997×10^{13}	6.664×10^{13}
	b^*	6.294×10^9	2.140×10^9	3.382×10^9	2.144×10^9	3.147×10^9
Recognized	AND	Yes	No	No	No	

^aThe target is object O1 under illuminant D65.

Table 5. Correlation and Discrimination Results Obtained from Multichannel Decomposition Expressed as Three Coefficients under Known Illuminant Conditions^a

Illuminant	Channel	Object				50% Threshold
		O1	O2	O3	O4	
D65	Coefficient 1	7.880×10^{-2}	5.710×10^{-2}	6.157×10^{-2}	5.828×10^{-2}	3.940×10^{-2}
	Coefficient 2	2.196×10^{-3}	1.142×10^{-5}	1.071×10^{-5}	2.400×10^{-3}	1.200×10^{-3}
	Coefficient 3	3.050×10^{-4}	4.342×10^{-5}	6.078×10^{-5}	1.103×10^{-4}	1.525×10^{-4}
Recognized	AND	Yes	No	No	No	
A	Coefficient 1	8.020×10^{-2}	5.896×10^{-2}	6.356×10^{-2}	5.997×10^{-2}	4.010×10^{-2}
	Coefficient 2	2.110×10^{-3}	1.064×10^{-5}	1.274×10^{-4}	2.291×10^{-3}	1.150×10^{-3}
	Coefficient 3	2.663×10^{-4}	3.140×10^{-5}	6.910×10^{-5}	9.648×10^{-5}	1.332×10^{-4}
Recognized	AND	Yes	No	No	No	
10,000K	Coefficient 1	7.690×10^{-2}	5.516×10^{-2}	6.013×10^{-2}	5.674×10^{-2}	3.845×10^{-2}
	Coefficient 2	2.400×10^{-3}	1.164×10^{-5}	9.621×10^{-5}	2.401×10^{-3}	1.200×10^{-3}
	Coefficient 3	2.995×10^{-4}	4.133×10^{-5}	6.622×10^{-5}	1.011×10^{-4}	1.497×10^{-4}
Recognized	AND	Yes	No	No	No	
Orange	Coefficient 1	8.060×10^{-2}	5.863×10^{-2}	6.270×10^{-2}	5.987×10^{-2}	4.030×10^{-2}
	Coefficient 2	2.180×10^{-3}	1.049×10^{-5}	1.122×10^{-4}	2.400×10^{-3}	1.200×10^{-3}
	Coefficient 3	2.838×10^{-4}	3.820×10^{-5}	5.989×10^{-5}	1.029×10^{-4}	1.419×10^{-4}
Recognized	AND	Yes	No	No	No	

^aThe target is object O1 under illuminant D65.

were measured by different authors^{24,31} was selected. The illuminant set included daylight spectra, incandescent lights, and lights with different color temperatures; we discarded the fluorescent illuminants to ensure that there would be a minimum number of three basis vectors in the following calculations.²³ $E_i(\lambda)$ were obtained through a PCA of these illuminants, and the dimension of the basis was fixed at $m = 3$; the first three eigenvectors are shown in Fig. 5(a). Then we used these basis functions in Eq. (7) to recover coefficient ε_i of each unknown illuminant condition under which the scene was captured. But how good is the illuminant estimation? Figure 5(b) shows an example of the linear recovery of test illuminant 4; in this figure we compare the theoretical and the estimated SPDs of the illuminants. The

original SPD of the illuminant was not known *a priori* in the correlation method and is shown here only to test the illuminant estimation hypothesis. To quantify the quality of the reconstructions we calculated the values of the goodness-of-fit coefficient (GFC), which measures the spectral similarities between the original and the estimated spectral functions, for these results. The GFC is based on Schwartz's inequality and is defined as

$$GFC = \frac{\left| \sum_j f(\lambda_j) f_r(\lambda_j) \right|}{\left[\sum_j [f(\lambda_j)]^2 \right]^{1/2} \left[\sum_j [f_r(\lambda_j)]^2 \right]^{1/2}}, \quad (9)$$

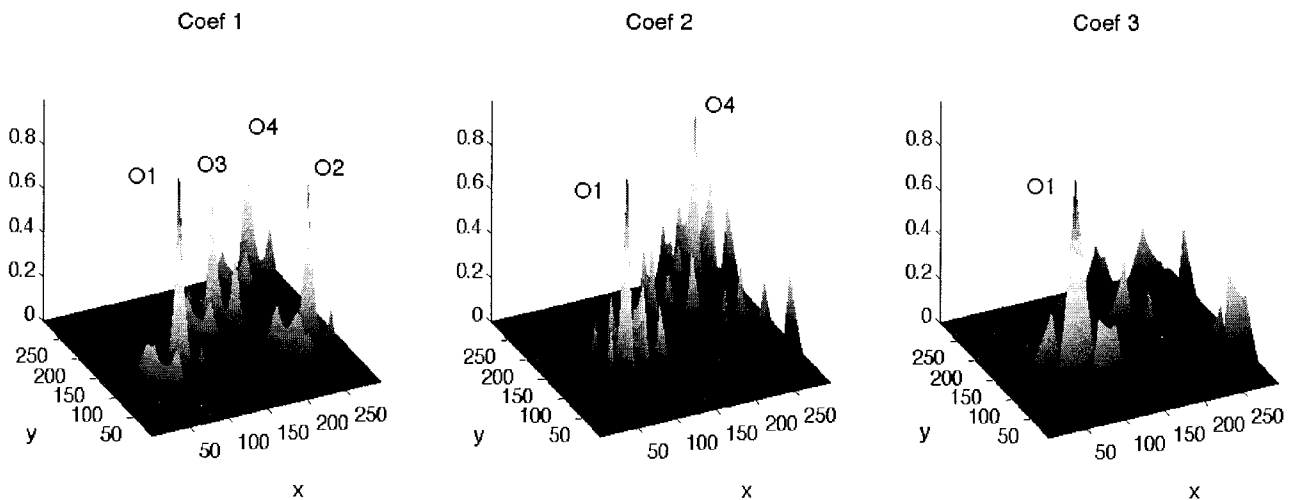


Fig. 3. Correlation peaks derived from coefficients σ_1^{xy} , σ_2^{xy} , and σ_3^{xy} when the scene was captured under illuminant A. The x and y coordinates represent spatial positions in the image. Correlation axes have been normalized in this figure for clarity.

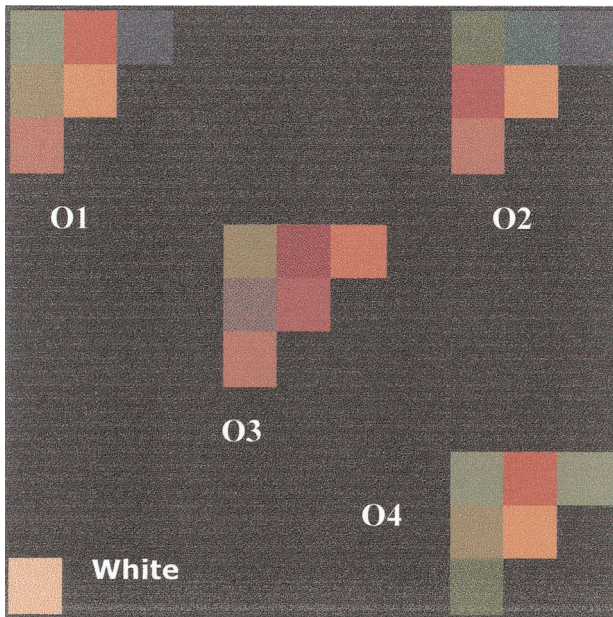


Fig. 4. Input color image captured under test illuminant 4. The white surface placed at the lower left corner of the scene was used for the illuminant-estimation hypothesis.

where $f(\lambda)$ and $f_r(\lambda)$ are the original and the estimated spectral functions, respectively. The GFC values runs from 0 to 1, so the mathematical reconstruction of the function would be better as the GFC values approach unity.^{23,32} We present in Table 6 the GFC values for the test illuminants used here. All the GFC values are close to 0.99, with the exception of that for illuminant 1, and an average GFC value of 0.9887 was obtained. Because the GFC is the multiple correlation coefficient R and the square root of the variance-accounted-for coefficient, this means that we have missed only approximately 2% of the energy in the reconstructions. Even though the spectral similarities between the original and the recovered spectral functions are not mathematically perfect, the recognition rates will not be severely affected by this fact, as we show below.

Next we used Eq. (8) to transform the color images under each of the unknown illuminants and to recover coefficients σ_j^{xy} . The correlation was performed between these coefficients and the corresponding coefficients of the target. The results are summarized in Tables 7–9 for the three multichannel techniques. On one hand, the results show the poor discrimination of the RGB multichannel correlation inasmuch as it identifies O1 and O4 as the targets for all the test illuminants. When we use the CIE Lab system the results are satisfactory and present false alarms for objects O1, O3, and O4 under test illuminant 4 only. On the other hand, the illuminant estimation hypothesis and the method of coefficients provide enough discrimination to permit O1 to be recognized under all the test illuminants, even though the color appearance of the target under reference illuminant D65 (O1 in the upper left corner of Fig. 1) was completely different from its correspond-

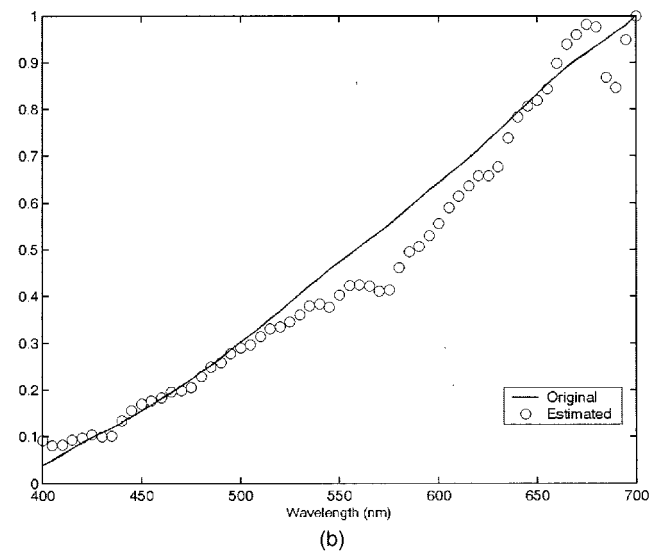
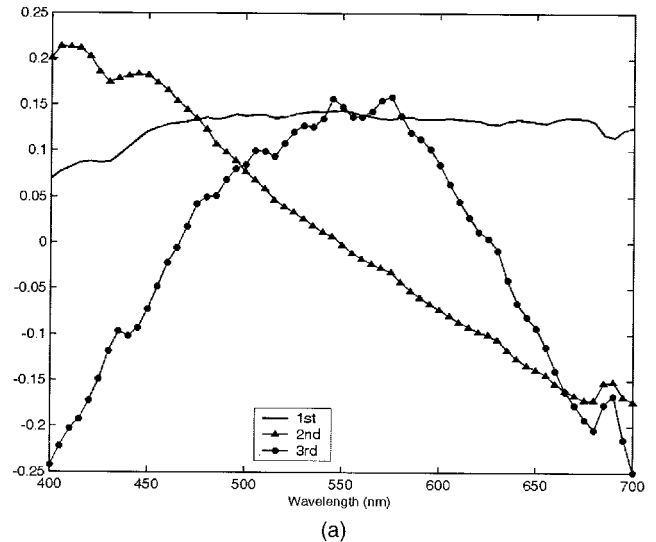


Fig. 5. (a) First three basis functions derived from PCA for the set of 83 illuminants used. (b) Original and estimated SPDs of test illuminant 4 derived from the illuminant-estimation algorithm.

ing image under each of the unknown illuminations (e.g., O1 in Fig. 4 under test illuminant 4). This result confirms the good discrimination capability of the proposed algorithm, independently of the spectral changes in the illumination. Figure 6 shows examples of the correlation results derived from the CIE Lab system and from coefficients σ_1^{xy} , σ_2^{xy} , and σ_3^{xy} when the source image was captured under one of the test illuminants.

Table 6. GFC and Root-Mean-Square Error Obtained for the Four Test Illuminants

Illuminant	GFC	Root-Mean-Square Error
1	0.9746	0.1685
2	0.9896	0.0964
3	0.9945	0.1087
4	0.9962	0.0567

Table 7. Correlation and Discrimination Results Obtained from Conventional RGB Multichannel Decomposition under Several Unknown Illuminant Conditions^a

Illuminant	Channel	Object				50% Threshold
		O1	O2	O3	O4	
Test 1	R	5.356×10^{14}	3.583×10^{14}	3.286×10^{14}	4.093×10^{14}	2.678×10^{14}
	G	3.506×10^{14}	1.893×10^{14}	1.513×10^{14}	3.882×10^{14}	1.941×10^{14}
	B	8.047×10^{13}	3.983×10^{13}	4.351×10^{13}	9.074×10^{13}	4.537×10^{13}
Recognized	AND	Yes	No	No	Yes	
Test 2	R	1.573×10^{14}	1.106×10^{14}	1.026×10^{14}	1.211×10^{14}	7.865×10^{13}
	G	2.614×10^{14}	1.408×10^{14}	1.179×10^{14}	2.888×10^{14}	1.444×10^{14}
	B	1.609×10^{14}	7.847×10^{13}	8.069×10^{13}	1.698×10^{14}	8.490×10^{13}
Recognized	AND	Yes	No	No	Yes	
Test 3	R	5.074×10^{14}	3.422×10^{14}	3.195×10^{14}	3.879×10^{14}	2.537×10^{14}
	G	5.098×10^{14}	2.741×10^{14}	2.233×10^{14}	5.644×10^{14}	2.822×10^{14}
	B	1.825×10^{14}	8.900×10^{13}	9.556×10^{13}	2.007×10^{14}	1.004×10^{14}
Recognized	AND	Yes	No	No	Yes	
Test 4	R	2.626×10^{14}	1.759×10^{14}	1.755×10^{14}	1.966×10^{14}	1.131×10^{14}
	G	9.639×10^{13}	5.274×10^{13}	4.263×10^{13}	1.059×10^{14}	5.296×10^{13}
	B	1.777×10^{13}	9.175×10^{12}	1.060×10^{13}	1.976×10^{13}	9.875×10^{12}
Recognized	AND	Yes	No	No	Yes	

^aThe target is object O1 under illuminant D65.

C. Color Object Discrimination under Outdoor Illumination

We show here an example of the correlation and discrimination results derived from an outdoor color scene. The source was the GretagMacbeth Color-Checker chart, and we captured it under daylight illumination. As shown in Fig. 7(a), the target was the color area O1, which corresponds to yellow chip number 16 of the ColorChecker chart, and the reference white was placed at the lower left corner of the scene, which coincides with chip number 19 of the color chart. The scene was captured under daylight

illumination on a clear day by a geometry that avoided the highlights in the image; the time exposure was adjusted before image capture to discard any saturated digital counts. The target and the source images were transformed independently according to Eq. (7), and the correlation described by multichannel Eq. (6) was obtained. Figure 7(b) resumes the discrimination results from each of coefficients σ_1^{xy} , σ_2^{xy} and σ_3^{xy} . The numbers in parentheses are the corresponding threshold values of 50% of the maximum correlation peaks. After the AND operator was applied to the three planes, the

Table 8. Correlation and Discrimination Results Obtained from Multichannel Decomposition Based on the CIE Lab Color Transformation under Several Unknown Illuminant Conditions^a

Illuminant	Channel	Object				50% Threshold
		O1	O2	O3	O4	
Test 1	L^*	1.534×10^{13}	1.249×10^{13}	1.190×10^{13}	1.359×10^{13}	7.669×10^{12}
	a^*	1.121×10^{14}	1.666×10^{13}	5.042×10^{13}	8.032×10^{13}	6.060×10^{13}
	b^*	7.522×10^9	2.991×10^9	4.368×10^9	3.332×10^9	3.771×10^9
Recognized	AND	Yes	No	No	No	
Test 2	L^*	1.412×10^{13}	1.159×10^{13}	1.064×10^{13}	1.348×10^{13}	7.062×10^{12}
	a^*	1.973×10^{14}	5.428×10^{13}	2.569×10^{13}	1.458×10^{14}	9.866×10^{13}
	b^*	8.708×10^9	3.164×10^9	3.705×10^9	3.646×10^9	4.354×10^9
Recognized	AND	Yes	No	No	No	
Test 3	L^*	1.300×10^{13}	1.059×10^{13}	9.963×10^{12}	1.281×10^{13}	6.502×10^{12}
	a^*	1.505×10^{14}	3.383×10^{13}	3.096×10^{13}	1.116×10^{14}	7.524×10^{13}
	b^*	7.274×10^9	2.719×10^9	3.668×10^9	3.329×10^9	3.637×10^9
Recognized	AND	Yes	No	No	No	
Test 4	L^*	1.492×10^{13}	1.217×10^{13}	1.216×10^{13}	1.435×10^{13}	7.461×10^{12}
	a^*	5.331×10^{13}	5.466×10^{13}	5.270×10^{13}	3.458×10^{13}	2.733×10^{13}
	b^*	6.154×10^9	3.056×10^9	3.785×10^9	3.370×10^9	3.077×10^9
Recognized	AND	Yes	No	Yes	Yes	

^aThe target is object O1 under the illuminant D65.

Table 9. Correlation and Discrimination Results Obtained from Multichannel Decomposition Expressed as Three Coefficients under Several Unknown Illuminant Conditions^a

Illuminant	Channel	Object				50%Threshold
		O1	O2	O3	O4	
Test 1	Coefficient 1	1.105×10^{-1}	8.050×10^{-2}	8.261×10^{-2}	8.371×10^{-2}	5.525×10^{-2}
	Coefficient 2	2.870×10^{-3}	2.135×10^{-5}	4.405×10^{-5}	3.110×10^{-3}	1.550×10^{-3}
	Coefficient 3	4.646×10^{-4}	6.796×10^{-5}	6.240×10^{-5}	1.853×10^{-4}	2.320×10^{-4}
Recognized	AND	Yes	No	No	No	
Test 2	Coefficient 1	9.854×10^{-2}	6.897×10^{-2}	7.295×10^{-2}	7.393×10^{-2}	4.925×10^{-2}
	Coefficient 2	2.740×10^{-3}	1.858×10^{-5}	1.104×10^{-4}	2.951×10^{-3}	1.500×10^{-3}
	Coefficient 3	4.230×10^{-4}	5.746×10^{-5}	5.595×10^{-5}	1.459×10^{-4}	2.115×10^{-4}
Recognized	AND	Yes	No	No	No	
Test 3	Coefficient 1	7.586×10^{-2}	5.408×10^{-2}	5.766×10^{-2}	5.656×10^{-2}	3.795×10^{-2}
	Coefficient 2	2.014×10^{-3}	1.462×10^{-5}	1.112×10^{-4}	2.172×10^{-3}	1.100×10^{-3}
	Coefficient 3	3.099×10^{-4}	4.198×10^{-5}	4.116×10^{-5}	1.137×10^{-4}	1.549×10^{-4}
Recognized	AND	Yes	No	No	No	
Test 4	Coefficient 1	9.616×10^{-2}	7.111×10^{-2}	7.481×10^{-2}	7.331×10^{-2}	4.810×10^{-2}
	Coefficient 2	2.418×10^{-3}	1.264×10^{-5}	1.552×10^{-4}	2.604×10^{-3}	1.300×10^{-3}
	Coefficient 3	3.621×10^{-4}	3.820×10^{-5}	5.628×10^{-5}	1.416×10^{-4}	1.810×10^{-4}
Recognized	AND	Yes	No	No	No	

^aThe target is object O1 under illuminant D65.

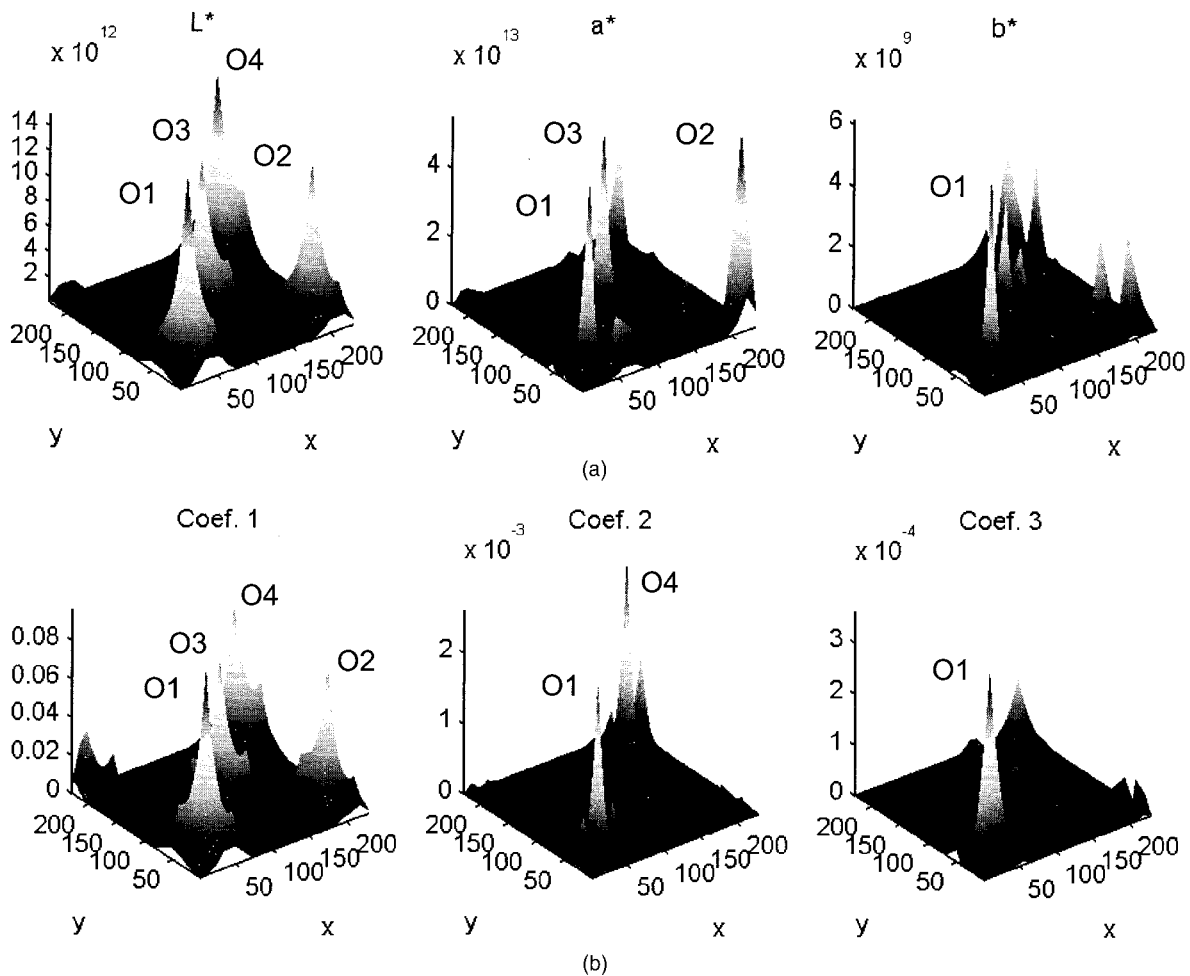


Fig. 6. (a) Correlation peaks derived from the CIELab coordinates when the scene was captured under test illuminant 4. The x and y coordinates represent spatial positions in the image. (b) Correlation peaks derived from coefficients $\sigma_{1^{xy}}$, $\sigma_{2^{xy}}$, and $\sigma_{3^{xy}}$ when the scene was captured under test illuminant 4. The x and y coordinates represent spatial positions in the image.

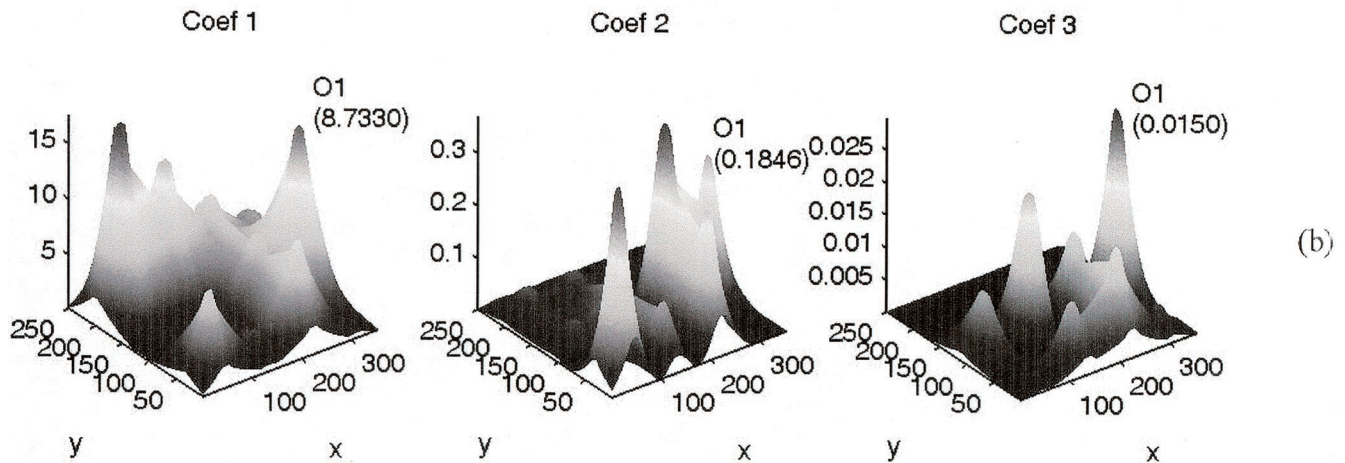
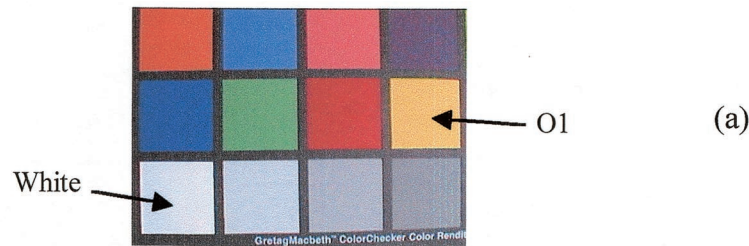


Fig. 7. (a) Image of the GretagMacbeth ColorChecker captured under daylight illumination. (b) Correlation peaks derived from coefficients σ_1^{xy} , σ_2^{xy} , and σ_3^{xy} ; the values of 50% of the maximum are shown in parentheses.

coefficient correlation method led to a positive discrimination of color object O1. Nevertheless, the correlation peaks are wider than those obtained in the examples above, and additional peaks appear around the target, although they do not lead to false alarms. This is so because the color areas are not so nearly spatially uniform as the simulated areas used in the scenes of Fig. 4. Two main reasons can explain these results: First, capturing color with a CCD is a noisy process, even when the camera is carefully calibrated and the dark noise is appropriately subtracted from the RGB values of each pixel; second, the results suggest that the linear models of reduced dimension used here probably do not suffice for an adequate description of surface reflectances. It will be important in future studies to analyze the use of multispectral object recognition with more than three coefficients, as we commented above, and its influence on the design of the matched filters used in the optical correlation architecture.

6. Conclusions

We have introduced what to our knowledge is a new method of multichannel decomposition of color images based on a linear description of spectral surfaces and illuminants that permits the introduction of color information in optical pattern recognition. The method uses linear models based on principal-component analysis to represent the spectral reflectance function of each image pixel and the spectral power distribution of the light sources in suitable

basis for linear representation. We first demonstrated the discrimination capability of the method under controlled illuminant conditions. The coefficient method can discriminate polychromatic objects, and the results are independent of any changes in the illuminant under which the scene is captured. The correlation results are satisfactory even for the low-dimensional basis used to represent the surface reflectance function of the image pixels. The discrimination capability of this method is clearly an improvement on that obtained with RGB multichannel decomposition and is slightly better than those of other approaches used in optical correlation, such as the CIE Lab system, that are based on uniform color spaces.

Also, we have demonstrated that optical color-pattern recognition can be achieved under conditions of unknown illuminants. In this case the use of a reference surface that is captured within the input color scene allows an illuminant-estimation algorithm to be used, which will lead to positive discrimination in situations when the target is captured under a reference illuminant and the scene containing the target is captured under an unknown, spectrally different illuminant. Although the recovered SPD of the illuminant was not mathematically perfect, the coefficient method provides reasonably good invariant color recognition. It is clear that the spectral recovery of surfaces and illuminants is limited by the dimensionality of the linear bases. More complicated and efficient algorithms can be used to esti-

mate the illumination. The small number of basis vectors used here, only three, is a compromise selection but allows us to illustrate the potential use of the method.

The results also suggest that the computation of only two of the coefficients (σ_2^{xy} and σ_3^{xy}) alone gives no false alarms between the source and the target images. But we believe that a potential use of the coefficient correlation method is precisely suited for the possibility of using more than three color components in optical pattern recognition, which can lead to better spectral surface description and accurate color object recognition. The linear description of both the source and the target color images leads to a multichannel correlation of a range as high as the dimension of the bases chosen to describe the surfaces and illuminants. The additional advantage of the coefficient correlation is that once the linear basis has been selected it allows the user to transform the input image into a subspace where the spatial information is preserved and the dependence on the spectral content of the illumination is discarded.

This study was supported by the Comisión Interministerial de Ciencia y Tecnología, Ministerio de Educación y Ciencia, Spain (grant BMF2000-1473).

References and Notes

1. F. T. S. Yu, "Color image recognition by spectral-spatial matched filtering," *Opt. Eng.* **23**, 690–695 (1984).
2. E. Badiqué, Y. Koyima, N. Ohyama, J. Tsujiuchi, and T. Honda, "Color image correlation," *Opt. Commun.* **61**, 181–186 (1987).
3. M. S. Millán, J. Campos, C. Ferreira, and M. J. Yzuel, "Matched filter and phase only filter performance in colour image recognition," *Opt. Commun.* **73**, 277–284 (1989).
4. M. S. Millán, M. J. Yzuel, J. Campos, and C. Ferreira, "Different strategies in optical recognition of polychromatic images," *Appl. Opt.* **31**, 2560–2567 (1992).
5. M.-L. Hsieh, K. Y. Hsu, and H. Zhai, "Color image recognition by use of a joint transform correlator of three liquid-crystal televisions," *Appl. Opt.* **41**, 1500–1504 (2002).
6. I. Moreno, V. Kober, V. Lashin, J. Campos, L. P. Yaroslavsky, and M. J. Yzuel, "Color pattern recognition with circular component whitening," *Opt. Lett.* **21**, 499–500 (1992).
7. M. S. Millán, M. Corbalán, J. Romero, and M. J. Yzuel, "Optical pattern recognition based on color vision models," *Opt. Lett.* **20**, 1722–1724 (1995).
8. A. Fares, P. García-Martínez, C. Ferreira, M. Hamdi, and A. Bouzid, "Multi-channel chromatic transformations for nonlinear color pattern recognition," *Opt. Commun.* **203**, 255–261 (2002).
9. J. Nicolas, M. J. Yzuel, and J. Campos, "Colour pattern recognition by three-dimensional correlation," *Opt. Commun.* **184**, 335–343 (2000).
10. J. Nicolas, I. Moreno, J. Campos, and M. J. Yzuel, "Phase-only filtering on the three-dimensional Fourier spectrum of color images," *Appl. Opt.* **42**, 1426–1433 (2003).
11. J. Nicolas, C. Iemmi, J. Campos, and M. J. Yzuel, "Optical encoding of color three-dimensional correlation," *Opt. Commun.* **209**, 35–43 (2002).
12. M. Corbalán, M. S. Millán, and M. J. Yzuel, "Color measurement in standard CIELAB coordinates using a 3CCD camera: correction for the influence of the light source," *Opt. Eng.* **39**, 1470–1476 (2000).
13. M. Corbalán, M. S. Millán, and M. J. Yzuel, "Color pattern recognition with CIELAB coordinates," *Opt. Eng.* **41**, 130–138 (2002).
14. M. J. Swain and D. H. Ballard, "Color indexing," *Int. J. Comput. Vision* **7**, 11–32 (1991).
15. B. V. Funt and G. D. Finlayson, "Color constant color indexing," *IEEE Trans. Pattern Anal. Mach. Intell.* **17**, 522–529 (1995).
16. G. D. Finlayson, S. D. Hordley, and P. M. Hubel, "Color by correlation: a simple, unifying framework for color constancy," *IEEE Trans. Pattern Anal. Mach. Intell.* **23**, 1209–1221 (2001).
17. L. Wang and G. Healey, "Using multiband filtered energy matrices for recognition and illumination correction," *Opt. Eng.* **37**, 2668–2674 (1998).
18. L. T. Maloney and B. Wandell, "Color constancy: a method for recovering surface spectral reflectance," *J. Opt. Soc. Am. A* **3**, 23–33 (1986).
19. A. García-Beltrán, J. L. Nieves, J. Hernández-Andrés, and J. Romero, "Linear bases for spectral reflectance functions of acrylic paints," *Color Res. Appl.* **23**, 39–45 (1998).
20. J. P. S. Parkinen, J. Hallikainen, and T. Jaaskelainen, "Characteristic spectra of Munsell colors," *J. Opt. Soc. Am. A* **6**, 318–322 (1989).
21. M. J. Vrhel, R. Gershon, and L. S. Iwan, "Measurements and analysis of object reflectance spectra," *Color Res. Appl.* **19**, 4–9 (1994).
22. E. R. Dixon, "Spectral distribution of Australian daylight," *J. Opt. Soc. Am.* **68**, 437–450 (1978).
23. J. Romero, A. García-Beltrán, and J. Hernández-Andrés, "Linear bases for representation of natural and artificial illuminants," *J. Opt. Soc. Am. A* **14**, 1007–1014 (1997).
24. J. Hernández-Andrés, J. Romero, J. L. Nieves, and R. L. Lee, Jr., "Color and spectral analysis of daylight in southern Europe," *J. Opt. Soc. Am. A* **18**, 1325–1335 (2001).
25. G. Buchsbaum, "A spatial processor model for object colour perception," *J. Franklin Inst.* **310**, 1–26 (1980).
26. M. D'Zmura and G. Iverson, "Color constancy. I. Basic theory of two-stage linear recovery of spectral descriptions for lights and surfaces," *J. Opt. Soc. Am. A* **10**, 2148–2165 (1993).
27. M. D'Zmura and G. Iverson, "Color constancy. II. Results from two-stage linear recovery of spectral descriptions for lights and surfaces," *J. Opt. Soc. Am. A* **10**, 2166–2180 (1993).
28. B. V. Funt, M. S. Drew, and J. Ho, "Color constancy from mutual reflection," *Int. J. Comput. Vision* **6**, 5–24 (1991).
29. See Ref. 13, pp. 1472–1475, for full details about the derivation of the matrices that allow the computation of CIE Lab coordinates from RGB values.
30. J. Y. Hardeberg, "Acquisition and reproduction of color images: colorimetric and multispectral approaches," Ph.D. dissertation (Ecole Nationale Supérieure des Télécommunications, Paris, 1999), pp. 157–174.
31. K. Barnard, L. Martin, B. Funt, and A. Coath, "A data set for color research," *Color Res. Appl.* **27**, 148–152 (2002).
32. F. H. Imai, M. R. Rosen, and R. S. Berns, "Comparative study of metrics for spectral match quality," in *Proceedings of the First European Conference on Colour in Graphics, Imaging, and Vision* (Society for Imaging Science and Technology, Springfield, Va., 2002), pp. 492–496.